Cell cycle follows "pause and play" mechanism in environment stress recovery in diverse plant species

Olivia S. Hazelwood[1], Kamryn A. Diehl[1], Vicky Hollenbeck[2], Dustin Herb[2], Joseph P. Gallagher[2,*], M. Arif Ashraf[1,*]

[1]Department of Botany, University of British Columbia, Vancouver, BC, Canada
[2]Forage Seed and Cereal Research Unit, United States Department of Agriculture, Corvallis, OR, USA

*Corresponding authors: M. Arif Ashraf (arif.ashraf@botany.ubc.ca); Joseph Gallagher (joseph.gallagher@usda.gov)

Abstract

Across the tree of life, organisms interact with the surrounding environment during growth and development. The alteration of organismal growth due to environmental stress is orchestrated at the cellular level and manifested at the organ level. Organismal growth relies on a combination of cell division, expansion, and differentiation. In a natural environment, periods of stress may be followed by recovery periods, when plants have the opportunity to return to normal growth conditions. We tested the cell cycle regulation during control, stress, and recovery period for salt, osmotic, cold, and heat stresses using eudicot *Arabidopsis thaliana* and monocots *Brachypodium distachyon* and *Lolium multiflorum* (annual ryegrass). We identified a conserved "pause and play" mechanism of cell cycle during environmental stress and recovery.

Keywords
Abiotic stress, Stress recovery, Cell cycle, AlphaFold, Plant development, Root growth

Environmental stresses, such as salinity, drought, cold, and heat, alter plant growth and development (*1*, *2*)**.** Plant growth is a combination of cell division, cell elongation, and cell differentiation (*3*, *4*). The reduction in growth during environmental stress response alters either the cell division, cell elongation, or both (*4*, *5*). How distinct environmental stresses target either cell division or elongation is still being unraveled. Furthermore, stress adaptation relies not only on survival during the stress period, but also on a plant's capacity to recover after stress conditions. Plant growth during the stress and stress recovery is orchestrated at the cellular level and manifests at the tissue and organ level. Cell cycle regulators control the cellular circuits important for both cell division and elongation and switch between these core functions and integrating environmental cues (*6*). A comparative genetics and cell biology approach for a wide range of environmental stresses and recovery could illustrate a fundamental mechanism important for plant adaptation, and, more broadly, an adaptive stress response for organisms. This understanding of stress response and recovery will allow us to connect the cellular regulators to the plant phenotypes they control.

Distinctive environmental stress and stress recovery response in plants

We investigated the root growth response of Arabidopsis (*Arabidopsis thaliana*) during environmental stresses and recovery periods. Firstly, we used the 4-day-old Arabidopsis root to measure both primary root length and cell length during the stress and recovery period (Fig. 1, A to F, and fig. S1). We observed ~40%, ~50%, 80% primary root growth inhibition for salt (48h), osmotic (mannitol) stress (48h), and cold (4°C) stress (24h), respectively, and 10% acceleration of primary root growth during heat (29°C) stress (24h) (Fig. 1, A to F, and fig. S1). It is not surprising that salt, osmotic, and cold stress inhibit the primary root growth, as numerous studies have demonstrated a similar phenomenon (*4*, *7*–*9*). At the same time, high temperature induced primary root growth acceleration has also been observed for Arabidopsis and other plant root systems (*10*–*13*).

In contrast to stress conditions, the outcome during the recovery period is surprising. Given an equal amount of time to recover following the stress condition, Arabidopsis root growth recovers from salt and cold stress (Fig. 1, A to D, and fig. S1) yet fail to recover from osmotic and heat stresses (Fig. 1, A,B,E,F, and fig. S1). Within 48h of transfer from the salt to control plates, Arabidopsis root starts growing similar to control recovery (Fig. 1, A and B). Similarly, cold-treated Arabidopsis roots require only 24h to recover 90% compared to the control recovery (Fig. 1, C and D). Given the importance of abiotic stress recovery in plants, we hypothesized that this recovery potential may be conserved beyond Arabidopsis. We tested the salt and cold stress recovery in two grasses – Brachypodium (*Brachypodium distachyon*) and annual ryegrass (*Lolium multiflorum*). Overall, root growth was more variable within these two species. Despite this higher variability, root growth rates still recover in Brachypodium and annual ryegrass during salt and cold stress recovery, although only cold stress recovery was significant (Fig.1, G to J, and fig. S1). In Brachypodium, the recovery from cold stress (~4 fold) is greater than salt stress recovery (~2 fold) (Fig.1, G to H), while in annual ryegrass, a similar salt (~1.5 fold) and cold (~1.5 fold) stress recovery pattern was

observed (Fig.1, I to J). This suggests that salt and cold stress recovery follow a shared mechanism across plant species. Because of differences in root architecture across these three species, a conserved cellular mechanism seems highly likely to control these changes in growth under stress and recovery.

Cell cycle mechanism during salt and cold stress recovery

The visible root growth during stress and recovery period happens through a combination of cell division and elongation (*3*–*5*). Cell division relies on a tightly regulated cell cycle, consisting of G1 (gap phase 1), S (DNA synthesis phase), G2 (gap phase 2), and M (mitosis). Molecular markers (CYCB1;1-GUS/GFP, Cytrap, PlaCCI, PCNA1-sGFP) in plants have been used for both visualization and quantification of cell cycle phases (*14*–*18*). In Arabidopsis, we utilized cell cycle markers Cytrap (indicates S/G2 and G2/M phases) and PCNA1-sGFP (highlights gap phase phase, early and late S) to quantify the cell cycle status and measured epidermal cell length to investigate the cell elongation. Both salt and osmotic stresses reduce the meristematic cell division activity and cell elongation (Fig. 2, A to F, and fig. S2). This data confirms the previous observation of reduced CYCB1;1-GUS activity during salt stress in Arabidopsis root (*19*). Interestingly, during the recovery period, both cell division and elongation, and consequently the root growth, recover for salt stress recovery, but not for osmotic stress recovery (Fig. 1, A to B, Fig. 2, A to F, and fig. S2). Previous studies on Arabidopsis and maize leaf during osmotic stress highlighted the importance of cell division activity as a key factor for growth revival during the rehydration stage (*20*, *21*).

Previously, we demonstrated that decreased root growth in cold stress is due to a decrease in G2/M phase cell cycle progression, and not due to a decrease in cell elongation (*4*). At the same time, more cells were observed in gap phase, visualized using PCNA-GFP, during cold stress (*4*). Here, we have observed that the cold stress recovery period is sufficient for root growth recovery, as well as to resume the cell cycle (Fig. 2, G to I, and fig. S3). Compared to other stress conditions, heat stressed plants demonstrate a faster root growth and an accelerated cell cycle during heat stress; however, they fail to recover like control conditions during the recovery period (Fig. 2, J to L, and fig. S3). Altogether, our data suggest that salt and cold stress recovery for root growth is tightly correlated with the cell cycle regulation (Fig. 2, A to L, and fig. S4). We further tested this concept using PCNA1-sGFP during salt stress and recovery period. Reminiscent of cold stress, more cells were observed in gap phase during salt stress, yet they resumed normal cell cycle patterns during the salt stress recovery (fig. S5). In Brachypodium, a similar pattern of reduced mitotic activity is observed due to salt stress (*22*). This quantitative cell biology approach during the stress and recovery period led us to conclude that the cell cycle follows a “pause and play” mechanism during the salt and cold stress recovery.

Salt and cold stress recovery require intact G1 to S and G2 to M transitions

To explore which genes might be regulating the observed changes in the cell cycle, we performed transcriptomics of Arabidopsis whole root tissue during stress (salt, osmotic,

138 cold, and heat) and recovery conditions (table S1). According to principal components
139 analysis, stress sample gene expression is typically distinct from control and recovery
140 sample gene expression (fig. S7). As expected, a low number of genes are differentially
141 expressed between the stress control and recovery control, while hundreds to
142 thousands of genes are differentially expressed between stress and recovery conditions
143 (fig. S6, table S2). Interestingly, a cluster of core Arabidopsis cell cycle genes is
144 differentially expressed during salt and cold stress and recovery (Fig. 3A, and fig. S8).
145 These genes are primarily divided into three major categories–cyclin dependent kinases
146 (CDKs), cyclins, and inhibitors (ICKs/KRPs) (*6*, *23*). CDKs, cyclins, and ICKs act in the
147 cell cycle in a phase-dependent manner. Relying on the existing literature to classify the
148 role of Arabidopsis core cell cycle proteins during G1 to S and G2 to M transitions (*6*),
149 we identified one CDK (CDKA;1) and two cyclins (CYCD1;1 and CYCD4;1) involved in
150 both G1 to S and G2 to M transitions (Fig. 3B, and fig. S9). Cyclins express transiently
151 during specific cell cycle phases and degrade after that period. In contrast, CDKs
152 remain stable during the cell cycle phase. As a result, we evaluated the role of CDKA;1
153 to block both G1 to S and G2 to M transitions. Unfortunately, *cdka;1* homozygous
154 mutant causes defect during the male gametophyte development (*24*).
155
156 To circumvent this issue, we took a chemical genetic approach and used olomoucine,
157 which inhibits CDKs in non-plant systems (fig. S10) (*25*–*27*). Before using the
158 olomoucine to block the cell cycle, we tried to understand the specificity of the
159 olomoucine by studying its interaction with CDKA;1 *in silico*. The AlphaFold3 predicted
160 structure of CDKA;1 (pLDDT = 90) was subjected to molecular dynamics simulations in
161 the presence of either ATP or olomoucine to assess whether CDKA;1's ATP-binding
162 site exhibits nonspecific affinity for other adenine-based ligands like olomoucine (*28*–
163 *31*). olomoucine binds to the same cleft of ATP-binding sites of CDKA;1 (Fig. 3C, fig.
164 S11, and movies S1, S2) (*32*, *33*). Additionally, molecular docking simulations predicted
165 binding affinities (Kd) of 4.3μM and 1.3μM with ATP and olomoucine, respectively. This
166 indicates that olomoucine binds more strongly to CDKA;1's ATP-binding site, and may
167 be able to out-compete ATP at lower concentrations. Since ATP binding with CDKA;1
168 happens in a reversible manner, we hypothesized that CDKA;1 inhibition caused by
169 olomoucine may also act in a reversible manner. We tested this possibility by treating
170 CDKA;1-mVenus/*cdka;1* transgenic line with olomoucine. Interestingly, the CDKA;1-
171 mVenus signal decreases dramatically after the olomoucine treatment and the signal re-
172 appears after a transfer to a control plate during the recovery period (Fig. 3, D to E).
173 Altogether, these findings demonstrate that olomoucine binds specifically and reversibly
174 to CDKA;1, validating its use as a targeted and reversible controllable tool for inhibiting
175 CDKA;1 activity *in planta*.
176
177 We performed the salt and cold recovery experiment in the presence of olomoucine
178 using Arabidopsis, Brachypodium, and annual ryegrass (Fig. 3, F to M). We created a
179 dose response curve for olomoucine and identified a critical concentration (15 μg/mL) to
180 inhibit ~50% root growth in Arabidopsis (fig. S9). In Arabidopsis, plants treated with
181 olomoucine had their growth reduced by ~50% and ~40% in salt and cold stress
182 recovery, respectively (Fig. 3, H to I). In Brachypodium and annual ryegrass, we see a
183 similar trend of growth reduction caused by olomoucine in the recovery phase, with the

184 mean root growth rate lower in olomoucine treated plants, except in the case of
185 Brachypodium salt recovery (Fig. 3, J to M). While these differences were not
186 significant, this may be due to the higher variability in root growth in the grasses, as
187 seen here and in other grass systems (Fig. 1, H and J, Fig. 3, J to M) (*34–36*). These
188 data suggest that intact G1 to S and G2 to M transitions are required for salt and cold
189 stress recovery across plant species.
190
191 **CDKA1-dependent cell cycle regulation is required during stress recovery**
192
193 Olomoucine-mediated CDKA;1 inhibition ensures a break in the G1 to S and G2 to M
194 transitions. But, it is hard to assess whether olomoucine targets any other cell cycle
195 regulators other than CDKA;1. To clarify this, we tried to find an *in vivo* cell cycle
196 inhibitor of CDKA;1. We relied on the previously published root single cell RNA
197 sequencing data and protein interaction data of CDKA;1 (*6*, *37*, *38*). ICK1 is one of the
198 cell cycle inhibitors identified as CDKA;1 interactor (*39*). Spatial expression of *CDKA;1*
199 (required for G1 to S and G2 to M transitions), *CYCB1;1* (G2 to M transition marker
200 gene), and *ICK1* demonstrated that both *CDKA;1* and *CYCB1;1* expression is
201 specifically high in the root apical meristem and reduces in the transitions and
202 elongation zone (Fig. 4A). In contrast, ICK1 expression is lower in the root apical
203 meristem region and higher in the transition and elongation zone (Fig. 4A). These data
204 clearly suggest a spatial regulation of *CDKA;1* and *ICK1* expression during the root
205 development. We performed a real time PCR using Arabidopsis roots to test the gene
206 expression of *CYCB1;1* , *CDKA1*, and *ICK1* during salt and cold stress, and stress
207 recovery conditions (Fig. 4, B to C). We found that *CYCB1;1* and *ICK1* gene
208 expressions are altered during the stress and recovery period (Fig. 4, B to C).
209 Compared to *CYCB1;1* and *ICK1* gene expression, the gene expression pattern for
210 *CDKA1* is not straightforward (Fig. 4, B to C). More importantly, the entire root was
211 used for the RNA isolation and cDNA preparation to perform the qPCR experiment,
212 where the spatial expression data is masked. Combining the existing single cell RNA
213 sequencing data with qPCR results, we suggest a stress and recovery specific altered
214 gene expression pattern of core cell cycle genes. Additionally, core cell cycle genes,
215 such as *CDKA1* may function at translational level. We hypothesized that
216 overexpression of *ICK1* will help to inhibit CDKA;1 and consequently block G1 to S and
217 G2 to M more specifically (Fig. 4D) (*40*). We tested this hypothesis by using *ICK1*
218 overexpression during salt and cold stress recovery. We found that *ICK1*
219 overexpression fails to recover during salt and cold stress recovery compared to wild-
220 type (Fig. 4, E to H). Altogether, our observation suggests that CDKA;1-dependent cell
221 cycle regulation to maintain proper G1 to S and G2 to M transitions is required for the
222 salt and cold stress recovery.
223
224 **Conclusions**
225
226 Our study revealed a cell cycle circuit required for environmental stress and recovery
227 mechanisms conserved across Arabidopsis, Brachypodium, and annual ryegrass,
228 species separated by 160 million years of evolution (*41*). This circuit relies on the
229 “pause and play” mechanism of the cell cycle during stress recovery that manifests as

root growth (Fig. 4I). Stress recovery is an important aspect of stress resilience that has not been widely considered in past studies, but the growth and performance of plants relies on post-stress recovery (*21*). Therefore this cell cycle regulation is important for both stress and subsequent recovery. We tested the discovery using a wide range of approaches – root growth response, cell biology approach through cell cycle markers, comparative transcriptomics, molecular biology, and chemical genetics (Fig. 4I). This can set a benchmark for studying stress and stress recovery in other plant systems. Root growth is a vital agricultural trait required for breeding and engineering crops with tolerance to environmental stresses (*42–45*). Many studies on environmental stresses focus on species-specific genes that confer individual stress tolerance. Here, we have found a pathway that is conserved across multiple plant species, and thus is likely conserved in other crop species. This mechanism provides a genetic framework for understanding the network of genes conferring salt and cold tolerance to flowering plants, and potentially other eukaryotic species.

Supplementary materials

Materials and methods

Plant materials

Arabidopsis thaliana accession Columbia (Col-0), *B. distachyon* Bd21-3, and *Lolium mutliflorum* 'Gulf' were used as wild types for experiments. The following lines were previously described: Cytrap (*15*), *pAtPCNA1::AtPCNA1-sGFP* (*17*), CDKA;1-mVenus/*cdka;1* (*46*), *35S::GFP-ICK1* (*40*).

Growth conditions

For Arabidopsis, seeds were surface sterilized with 1mL 70% ethanol for 10 minutes, washed twice with 1mL autoclaved MQ water inside the laminar flow hood, and placed on the surface of ½ Murashige and Skoog (MS) media (BioWorld; Cat.# 30630058) containing 1% sucrose (BioWorld; Cat.# 41900152) and 1% agar (BioWorld; Cat.# 40100072) in square petri dishes (Simport; Cat.# 26-275). Plate openings were sealed with micropore tapes (Amazon; 3M A-1530-0 Micropore Surgical Tape, ½ Inch), covered with aluminum foil, and kept at 4°C for 2 days. After 2 days, plates are placed vertically under constant light conditions at 22°C.

For *B. distachyon*, seeds were surface sterilized with 0.6% NaOCl, 0.1% Tween-20 for 7 minutes shaking at 200 rpm, washed three times with autoclaved E-pure water inside a laminar flow hood, and left to soak at 4°C for 7 days. Imbibed seeds were placed on the surface of ½ MS media containing 1% sucrose and 1% agar. Plates were sealed with parafilm and oriented vertically under constant light at 22°C.

For *L. multiflorum*, seeds were dehusked in 50% sulfuric acid for 15 minutes, shaking at 200 rpm. Dehusked seeds were rinsed with 500 ml autoclaved E-pure water in a sterile Gooch crucible in the laminar flow hood. Then seeds were sterilized with 3.75% NaOCl, 0.1% Tween-20 for 20 minutes shaking at 200 rpm, rinsed with 500 ml autoclaved E-pure water in a sterile Gooch crucible in the laminar flow hood, and placed on the surface of ½ MS media containing 1% sucrose and 1% agar. Plates were sealed with parafilm and oriented vertically under constant light at 22°C.

Stress and stress recovery conditions

Stress and recovery conditions and timeline is summarized in Suppl Fig 1. For the Arabidopsis salt and osmotic stresses, 100mM NaCl and 300mM mannitol-containing ½ MS plates were used, respectively, to incubate seedlings for 2 days. Cold and heat stresses were performed using 4°C and 29°C chambers, respectively, for 1 day period. During the salt and osmotic stress recovery, seedlings were transferred to control media for 2 days. For cold and heat recovery, seedlings were returned to control growth temperature for 1 day period. Standard Arabidopsis growth conditions were maintained in a growth shelf with constant light conditions.

Two days after germination, Brachypodium and annual ryegrass seedlings were incubated in stress conditions for 48 hrs. Seedlings in control conditions were incubated

322 on ½ MS media plates at 22°C under constant light, seedlings under salt stress
323 conditions were incubated on 200 mM NaCl ½ MS media plates under control
324 temperature and light conditions, and seedlings under cold stress conditions were
325 incubated at 4°C in control media and light conditions. After stress conditions, seedlings
326 were moved to new ½ MS media plates at 22°C under constant light for 48 hrs for
327 stress recovery. All experiments took place in Percival or Conviron growth chambers.
328
329 **Phenotypic image analysis**
330 Images of Arabidopsis, Brachypodium, and annual ryegrass root growth were obtained
331 using the Epson Perfection V600 Photo scanner (Ver. 3.9.3.1) at 300 dpi in .TIFF
332 format. Root length was measured using open source ImageJ/Fiji software (*47*). Plant
333 growth was recorded before stress, after stress, and after stress recovery.
334
335 **Drug treatments**
336 Olomoucine (Cayman Chemical, Cat.# 10010240) was dissolved in DMSO and
337 incorporated into ½ MS media at various concentrations for dose response assay.
338
339 For olomoucine recovery inhibition experiments, seedlings and stress conditions were
340 the same as described for stress and recovery experiments above. For the stress
341 recovery period, seedlings were either placed on control ½ MS media or ½ MS media
342 with 15 µg/ml olomoucine. Images and measurements were taken as described above.
343
344 **Microscopic imaging**
345 Epidermal cell length was observed using a 20x objective lens attached with a Leica DM
346 2000 LED compound microscope setup and the images were taken by Leica MC170
347 HD camera attached with the Leica DM 2000 LED.
348
349 Epidermal cell length was also observed with a 20x objective lens attached with
350 AmScope T490 Series Simul-Focal Biological Trinocular Compound Microscope and
351 images were captured using a 18MP USB 3.0 C-mount Camera and AmScope
352 software.
353
354 The cell cycle regulation during control, stress, and stress recovery was measured
355 through cell cycle marker, Cytrap, which indicates S/G2 and G2/M states of cell cycle
356 using *pHTR2::CDT1a (C3)-RFP* and *pCYCB1::CYCB1-GFP*, respectively(*15*). The G1,
357 S, and G2 phase of the cell cycle was visualized using *pAtPCNA1::AtPCNA1-sGFP* (*17*)
358 during control, salt stress, and salt recovery conditions. Fluorescent images of live
359 Arabidopsis root meristem were imaged using a Nikon Ti-E-PFS inverted spinning-disk
360 confocal microscope equipped with x20 (Cytrap) and x40 silicone oil immersion
361 (*pAtPCNA1::AtPCNA1-sGFP*) objectives. The system is outfitted with a Yokogawa
362 CSU-X1 spinning disk unit, a self-contained 4-line laser module (excitation at 405, 488,
363 561, and 640 nm), and Andor iXon 897 EMCCD camera. 488nm and 561nm excitation
364 were used for GFP and RFP, respectively. Fluorescent images were acquired using the
365 Nikon NIS-Elements software and processed using ImageJ software (imagej.nih.gov/ij/).
366 Cells in both the longitudinal (meristematic region) and radial (the entire Z axis)
367 dimensions of root were counted for both Cytrap and *pAtPCNA1::AtPCNA1-sGFP* roots.

368
369 CDKA;1-mVenus images were acquired using an Olympus IXplore SpinSR system
370 (Evident, Tokyo, Japan), equipped with an inverted microscope (IX83; Evident, Japan),
371 a CSUW1-Sora spinning disk confocal unit (Yokogawa, Japan) and a Hamamatsu
372 ORCA Fusion BT camera. Fluorescence images were obtained with a 20x objective
373 (UPLXAPO 20X/0.8NA) and fluorescent signals from CDKA;1-mVenus were detected
374 with 514 nm excitation and 500-550 nm emission. Fluorescence confocal images were
375 acquired using software cellSens (Evident, Tokyo, Japan).
376
377 **RNA-seq**
378 RNA Isolation was performed using Arabidopsis Col-0 roots for control, stress (salt,
379 osmotic, cold, and heat), and stress recovery conditions using Qiagen RNeasy Plant
380 Mini Kit (Cat.# 74904). The extracted RNA concentration and quality was analyzed
381 using Thermo Scientific NanoDrop One (Cat.# 13-400-518). A total of 48 RNA samples
382 (4 stresses X 3 conditions X 3 biological replicates) were considered for the experiment.
383 Poly-A enriched RNA-seq libraries were prepared by using Vazyme VAHTS Universal
384 V10 RNA-seq Library Prep Kit and sequenced at 150-bp PE on an Element AVITI
385 instrument by AmpSeq (Gaithersburg, Maryland, USA) (https://www.ampseq.com/).
386 Reads were filtered with fastp v0.23.1 (*48*), mapped with STAR v2.7.11 to the TAIR10
387 Arabidopsis genome (*49*, *50*), and quantified with Salmon v1.10.2 (*51*). Four samples
388 were outliers and excluded from analysis. Differential gene expression was called at
389 FDR<0.05 with package DESeq2 v1.44.0 in R (*52*, *53*) and visualized with package
390 pheatmap v1.0.12 (*54*).
391
392 **Analyzing single cell sequencing data**
393 *CYCB1;1*, *CDKA;1*, and *ICK1* gene expression was visualized using Trevor Nolan's lab
394 (https://shiny.mdc-berlin.de/ARVEX/) and Root Cell Atlas (https://rootcellatlas.org/)
395 visualization tools for already published single cell sequencing data of Arabidopsis root.
396
397 **qPCR**
398 Each RNA concentration was normalized with RNase-free water, and 500 ng RNA was
399 used to synthesize cDNA using NEB ProtoScript II Reverse Transcriptase (Cat.#
400 M0368S). Quantitative PCR reactions were performed using StepOnePlus Real-Time
401 PCR System (Applied Biosystems) and PowerUp SYBR Green Master Mix (Applied
402 Biosystems; Cat.# A25741). The reaction was performed as per the manufacturer's
403 instructions. The list of primers used in this study is mentioned in Supplemental Table 3.
404
405 **Molecular docking and simulation**
406 Structural models of CDKA1 bound to ATP and olomoucine were predicted using the
407 AlphaFold Server (*28*) and DynamicBind (*29*) via the Neurosnap Inc web servers
408 (https://neurosnap.ai/). Molecular dynamics simulations were conducted using
409 GROMACS (*30*). Parameters included the AMBER99SB-ILDN force field, a cubic
410 solvent box with an ionic concentration of 0.15 M over a 1 nanosecond simulation time.
411 All simulations were carried out using the Neurosnap Inc server (https://neurosnap.ai/).
412 Simulation H-bond occupancies were analyzed using Galaxy Cheminformatics web
413 servers, with an angle cutoff of 20 degrees and distance cutoff of 3 Ångstroms (*55*, *56*).

Molecular visualization and structural rendering of CDKA1 and ligands were performed using ChimeraX 1.4 (*31*).

Statistical analysis

The raw data for each quantification was imported to statistical software JMP Pro17 for generating graphs and performing statistical tests.

Acknowledgements

The authors thank Masaaki Umeda (Nara Institute of Science and Technology), Sachihiro Matsunaga (Tokyo University of Science), Arp Schnittger (University of Hamburg), and Hong Wang (University of Saskatchewan) for sharing Cytrap (1), *pAtPCNA1::AtPCNA1-sGFP* (2), CDKA;1-mVenus/*cdka;1* (3), and *35S::GFP-ICK1* (4), respectively, seeds. Authors thank Miki Fujita and EunKyoung Lee of UBC Bioimaging Facility (RRID: SCR_021304) for their kind support.

Funding

The research at Ashraf lab is funded by the start-up grant provided by the Department of Botany and Faculty of Science at the University of British Columbia. Research in Gallagher and Herb labs is supported by the US Department of Agriculture Agricultural Research Service (2072-21500-001-000D).

Authors contributions

O.S.H., K.A.D., V.H., D.H., J.P.G., M.A.A. designed and performed experiments and analyzed data. O.S.H., J.P.G., and M.A.A. wrote the manuscript and all the authors agreed with the final version of the manuscript.

Competing interests

Authors declare no conflict of interests.

Figure legends

Figure 1: Environmental stress and stress recovery in Arabidopsis, Brachypodium, and annual ryegrass. (A) Root growth response of Arabidopsis in presence of salt and mannitol stress (upper panel) and recovery (lower panel). (B) Quantification of root growth from A. (C) Root growth response of Arabidopsis during pre- and post-cold stress, and post-cold stress recovery conditions. (D) Quantification of root growth from C. (E) Root growth response of Arabidopsis during pre- and post-heat stress, and post-heat stress recovery conditions. (F) Quantification of root growth from E. (G) Examples of root growth response of Brachypodium during salt and cold stress, and consequent recovery period. (H) Quantification of Brachypodium root growth in salt and cold stress and recovery experiments. (I) Examples of root growth response of annual ryegrass during salt and cold stress, and consequent recovery period. (J) Quantification of annual ryegrass root growth in salt and cold stress and recovery experiments.In panels A, C, E, G, and I, scale bar = 10 mm. Statistical test is performed based on Tukey's Honest test (B, D, F, H, and J). Groups labeled with the same letter are not statistically different

460 from each other (alpha = 0.05). Boxplots show median values (center line), 25th to 75th
461 interquartile range (box) and 1.5*interquartile range (whiskers) (B, D, F, H, and J).
462
463 **Figure 2:** Response of cell cycle marker during environmental stress and stress
464 recovery in Arabidopsis. Representative images of cell cycle marker Cytrap,
465 quantification of S/G2 and G2/M phase specific cells, and cell cycle regulation model
466 during salt (A-C), osmotic (D-F), cold (G-I), and heat (J-L) stress and recovery periods.
467 Magenta and green indicate S/G2 and G2/M phase, respectively, specific cells. At least
468 8-10 roots were observed for each condition and the entire Z plane of the root meristem
469 was considered to quantify the cells. Scale bar = 100 µm (A, D, G, and J). Statistical
470 test is performed based on Tukey's Honest test (B, E, H, and K). Groups labeled with
471 the same letter are not statistically different from each other (alpha = 0.05). Boxplots
472 show median values (center line), 25th to 75th interquartile range (box) and
473 1.5*interquartile range (whiskers) (B, E, H, and K).
474
475 **Figure 3:** Intact G1 to S and G2 to M transitions are required for salt and cold stress
476 recovery. (A) Relative expression of a sub-set of core cell cycle genes during the salt
477 and cold stress, and subsequent recovery periods. (B) List of Arabidopsis CDKs
478 involved in G1 to S (yellow) and G2 to M (cyan) transitions. (C) *In silico* interaction
479 assay of olomoucine (left, red) and ATP (right, magenta) with CDKA1 (cyan). Interacting
480 amino acids were highlighted in yellow. (D) CDKA;1-mVenus signal in presence of
481 olomoucine and the recovery period. (E) Quantification of mean gray value from D. Salt
482 (F) and cold (G) stress recovery in presence of olomoucine in Arabidopsis.
483 Quantification of salt (H) and cold (I) stress recovery in presence of olomoucine from F
484 and G, respectively. Salt (J) and cold (K) stress recovery in presence of olomoucine in
485 Brachypodium. Salt (L) and cold (M) stress recovery in presence of olomoucine in
486 annual ryegrass. Scale bar = 100 µm (D) and 10 mm (F and G). (E) Statistical test is
487 performed based on Tukey's Honest test. Groups labeled with the same letter are not
488 statistically different from each other (alpha = 0.05). Boxplots show median values
489 (center line), 25th to 75th interquartile range (box) and 1.5*interquartile range
490 (whiskers). Student's t-test was performed for H, I, J, K, L, and M.
491
492 **Figure 4:** CDKA1-dependent cell cycle transitions are required for salt and cold stress
493 recovery. (A) Single cell sequencing data for demonstrating the spatial expression
494 pattern of *CYCB1;1* (left), *CDKA1* (middle), and *ICK1* (right). The upper panel highlights
495 a color based gradient for longitudinal expression pattern and the lower panel highlights
496 the expression pattern in a dot plot manner. Real time PCR of *CYCB1;1* (left), *CDKA1*
497 (middle), and *ICK1* (right) genes in salt (B) and cold (C) stress, and corresponding
498 recovery periods. (D) Schematic model of ICK1 overexpression based CDK inhibition.
499 Salt (E) and cold (F) recovery response of ICK1 overexpression line in Arabidopsis.
500 Quantification of root growth response of ICK1 overexpression line during salt (G) and
501 cold (H) stress and recovery from E and F, respectively. (I) Graphical model highlights
502 the summarized version of the study, where Arabidopsis, Brachypodium, and annual
503 ryegrass were tested for multiple stress, and stress recovery focusing on cell cycle
504 regulation at organ or root growth, cellular, and molecular scale. Scale bar = 10 mm (E
505 and F). Statistical test is performed based on Tukey's Honest test (B, C, G, and H).

506 Groups labeled with the same letter are not statistically different from each other (alpha
507 = 0.05). Boxplots show median values (center line), 25th to 75th interquartile range
508 (box) and 1.5*interquartile range (whiskers) (B, C, G, and H).
509
510 **Supplemental figure 1:** Experimental conditions for Arabidopsis, Brachypodium, and
511 annual ryegrass. Concentration of salt and mannitol, temperature for cold and heat
512 stress, and developmental stage of root, and incubation periods were mentioned for
513 each individual stress and each organism used in this study.
514
515 **Supplemental figure 2:** Cell elongation during salt and osmotic stress, and stress
516 recovery period. (A) Epidermal cell length was measured during the control, salt and
517 osmotic stress, and corresponding recovery period. Scale bar = 100 μm. (B)
518 Quantification of cell length from A. Statistical test is performed based on Tukey's
519 Honest test. Groups labeled with the same letter are not statistically different from each
520 other (alpha = 0.05). Boxplots show median values (center line), 25th to 75th
521 interquartile range (box) and 1.5*interquartile range (whiskers).
522
523 **Supplemental figure 3:** Cell elongation during cold and heat stress, and stress
524 recovery period. (A) Epidermal cell length was measured during the control, cold and
525 heat stress, and corresponding recovery period. Scale bar = 100 μm. (B) Quantification
526 of cell length from A. Statistical test is performed based on Tukey's Honest test. Groups
527 labeled with the same letter are not statistically different from each other (alpha = 0.05).
528 Boxplots show median values (center line), 25th to 75th interquartile range (box) and
529 1.5*interquartile range (whiskers).
530
531 **Supplemental figure 4:** Summary of cell division and cell elongation during salt,
532 osmotic, cold, and heat stress, and stress recovery period. The summary is based on
533 Figure 1, 2, and Supplemental figure 2, 3. Upward and downward arrow during stress
534 condition indicates increased cell division or cell elongation. Dash line indicates neutral
535 or wild-type response to the stress. Tick and cross marks indicate recovered and not
536 recovered cell division or cell elongation during the recovery period. Dash line indicates
537 neutral or wild-type response during the recovery period.
538
539 **Supplemental figure 5:** PCNA-GFP signal during salt stress and recovery. (A) Cell
540 cycle marker PCNA-GFP signal during salt stress and recovery. Scale bar = 100 μm.
541 (B) Characteristic pattern of whole (Gap phase), dotted (early S phase), and speckled
542 (late S phase) pattern of PCNA-GFP marker. (C) Quantification of number of cells in
543 gap phase and S phase during salt stress and recovery. Statistical test was performed
544 based on Fisher's exact test.
545
546 **Supplemental figure 6:** Differential gene expression from comparative transcriptomics.
547 Number of differentially expressed genes during stress [salt (A), osmotic (A), cold (B),
548 and heat (B)] and stress recovery are highlighted.
549
550 **Supplemental figure 7:** Principal component analysis (PCA) of RNAseq samples. PCA
551 demonstrates the clustering of similar RNAseq samples for control, stress, control

552 recovery, and stress recovery in A (salt and osmotic stress) and B (cold and heat
553 stress).
554
555 **Supplemental figure 8:** Differential expression of core cell cycle genes in Arabidopsis.
556 Log2Fold changes of core cell cycle genes based on the comparative transcriptomics
557 during salt and cold stress, and stress recovery. The gene clustering highlights a subset
558 of genes used in Figure 3A.
559
560 **Supplemental figure 9:** Cell cycle specific function of CDKs and cyclins. List of
561 Arabidopsis CDKs and cyclins involved in G1 to S (yellow) and G2 to M (cyan)
562 transitions.
563
564 **Supplemental figure 10:** Dose response curve of olomoucine. (A) Quantification of root
565 length in presence of 1, 5, 10, 12.5, 25, and 50 µg/ml olomoucine. (B) Representative
566 images for each olomoucine concentration corresponding to A. Scale bar = 10 mm.
567
568 **Supplemental figure 11:** Hydrogen bond occupancy of ATP and olomoucine with
569 CDKA1. Interacting amino acids responsible for maintaining interaction with CDKA1 for
570 both ATP and olomoucine; and hydrogen bond occupancy for each interaction.
571
572 **Supplemental Table 1:** Read counts for RNA-seq libraries.
573
574 **Supplemental Table 2:** Differentially expressed genes in RNA-seq experiment.
575
576 **Supplemental Table 3:** List of primers used in this study for qPCR experiment.
577
578 **Supplemental movie 1:** Molecular dynamic simulation of CDKA;1 (cyan) and
579 olomoucine (red). The interacting amino acid residues are highlighted in yellow.
580
581 **Supplemental movie 2:** Molecular dynamic simulation of CDKA;1 (cyan) and ATP
582 (magenta). The interacting amino acid residues are highlighted in yellow.
583
584
585 **References and Notes**
586
587 1. H. Zhang, J. Zhu, Z. Gong, J.-K. Zhu, Abiotic stress responses in plants. *Nat Rev*
588 *Genet* **23**, 104–119 (2022).

589 2. J.-K. Zhu, Abiotic Stress Signaling and Responses in Plants. *Cell* **167**, 313–324
590 (2016).

591 3. A. Rahman, A. Bannigan, W. Sulaman, P. Pechter, E. B. Blancaflor, T. I. Baskin,
592 Auxin, actin and growth of the Arabidopsis thaliana primary root. *The Plant Journal*
593 **50**, 514–528 (2007).

594 4. M. A. Ashraf, A. Rahman, Cold stress response in Arabidopsis thaliana is mediated
595 by GNOM ARF-GEF. *The Plant Journal* **97**, 500–516 (2019).

596 5. M. A. Ashraf, T. Akihiro, K. Ito, S. Kumagai, R. Sugita, K. Tanoi, A. Rahman, ATP
597 binding cassette proteins ABCG37 and ABCG33 function as potassium-independent
598 cesium uptake carriers in Arabidopsis roots. *Molecular Plant* **14**, 664–678 (2021).

599 6. A. Shimotohno, S. S. Aki, N. Takahashi, M. Umeda, Regulation of the Plant Cell
600 Cycle in Response to Hormones and the Environment. *Annual Review of Plant*
601 *Biology* **72**, 273–296 (2021).

602 7. W. Feng, D. Kita, A. Peaucelle, H. N. Cartwright, V. Doan, Q. Duan, M.-C. Liu, J.
603 Maman, L. Steinhorst, I. Schmitz-Thom, R. Yvon, J. Kudla, H.-M. Wu, A. Y. Cheung,
604 J. R. Dinneny, The FERONIA Receptor Kinase Maintains Cell-Wall Integrity during
605 Salt Stress through Ca2+ Signaling. *Current Biology* **28**, 666-675.e5 (2018).

606 8. S. Gonzalez, J. Swift, J. Xu, N. Illouz-Eliaz, J. R. Nery, J. R. Ecker, Mimicking
607 genuine drought responses using a high throughput plate assay. *eLife* **12** (2023).

608 9. Q. Feng, S. Song, Y. Yang, M. Amee, L. Chen, Y. Xie, Comparative physiological and
609 metabolic analyzes of two Italian ryegrass () cultivars with contrasting salinity
610 tolerance. *Physiologia Plantarum* **172**, 1688–1699 (2021).

611 10. N. Takahashi, N. Ogita, T. Takahashi, S. Taniguchi, M. Tanaka, M. Seki, M. Umeda,
612 A regulatory module controlling stress-induced cell cycle arrest in Arabidopsis. *eLife*
613 **8**, e43944 (2019).

614 11. H. Ai, J. Bellstaedt, K. S. Bartusch, L. Eschen-Lippold, S. Babben, G. U. Balcke, A.
615 Tissier, B. Hause, T. G. Andersen, C. Delker, M. Quint, Auxin-dependent regulation
616 of cell division rates governs root thermomorphogenesis. *The EMBO Journal* **42**,
617 e111926 (2023).

618 12. T. Hanzawa, K. Shibasaki, T. Numata, Y. Kawamura, T. Gaude, A. Rahman,
619 Cellular Auxin Homeostasis under High Temperature Is Regulated through a
620 SORTING NEXIN1–Dependent Endosomal Trafficking Pathway. *The Plant Cell* **25**,
621 3424–3433 (2013).

622 13. S. Parveen, A. Rahman, Actin Isovariant ACT7 Modulates Root
623 Thermomorphogenesis by Altering Intracellular Auxin Homeostasis. *International*
624 *Journal of Molecular Sciences* **22**, 7749 (2021).

625 14. A. Colón-Carmona, R. You, T. Haimovitch-Gal, P. Doerner, Spatio-temporal
626 analysis of mitotic activity with a labile cyclin–GUS fusion protein. *The Plant Journal*
627 **20**, 503–508 (1999).

628 15. K. Yin, M. Ueda, H. Takagi, T. Kajihara, S. Sugamata Aki, T. Nobusawa, C. Umeda-
629 Hara, M. Umeda, A dual-color marker system for in vivo visualization of cell cycle
630 progression in Arabidopsis. *The Plant Journal* **80**, 541–552 (2014).

631 16. B. Desvoyes, A. Arana-Echarri, M. D. Barea, C. Gutierrez, A comprehensive
632 fluorescent sensor for spatiotemporal cell cycle analysis in Arabidopsis. *Nat. Plants*

633 **6**, 1330–1334 (2020).

634 17. R. Yokoyama, T. Hirakawa, S. Hayashi, T. Sakamoto, S. Matsunaga, Dynamics of
635 plant DNA replication based on PCNA visualization. *Sci Rep* **6**, 29657 (2016).

636 18. O. S. Hazelwood, M. A. Ashraf, Molecular markers in cell cycle visualisation during
637 development and stress conditions in Arabidopsis thaliana. *Quantitative Plant*
638 *Biology* **5**, e14 (2024).

639 19. G. West, D. Inzé, G. T. S. Beemster, Cell Cycle Modulation in the Response of the
640 Primary Root of Arabidopsis to Salt Stress. *Plant Physiology* **135**, 1050–1058
641 (2004).

642 20. A. Skirycz, H. Claeys, S. De Bodt, A. Oikawa, S. Shinoda, M. Andriankaja, K.
643 Maleux, N. B. Eloy, F. Coppens, S.-D. Yoo, K. Saito, D. Inzé, Pause-and-Stop: The
644 Effects of Osmotic Stress on Cell Proliferation during Early Leaf Development in
645 Arabidopsis and a Role for Ethylene Signaling in Cell Cycle Arrest. *The Plant Cell*
646 **23**, 1876–1888 (2011).

647 21. T. Van Hautegem, H. Takasaki, C. D. Lorenzo, K. Demuynck, H. Claeys, T. Villers,
648 H. Sprenger, K. Debray, D. Schaumont, L. Verbraeken, J. Pevernagie, J. Merchie,
649 B. Cannoot, S. Aesaert, G. Coussens, K. Yamaguchi-Shinozaki, M. L. Nuccio, F.
650 Van Ex, L. Pauwels, T. B. Jacobs, T. Ruttink, D. Inzé, H. Nelissen, Division Zone
651 Activity Determines the Potential of Drought-Stressed Maize Leaves to Resume
652 Growth after Rehydration. *Plant, Cell & Environment* **48**, 1242–1258 (2025).

653 22. E. Wolny, A. Skalska, A. Braszewska, L. A. J. Mur, R. Hasterok, Defining the Cell
654 Wall, Cell Cycle and Chromatin Landmarks in the Responses of Brachypodium
655 distachyon to Salinity. *International Journal of Molecular Sciences* **22**, 949 (2021).

656 23. Y. Cheng, H. Liu, L. Cao, S. Wang, Y. Li, Y. Zhang, W. Jiang, Y. Zhou, H. Wang,
657 Down-regulation of multiple CDK inhibitor ICK/KRP genes promotes cell
658 proliferation, callus induction and plant regeneration in Arabidopsis. *Front. Plant Sci.*
659 **6** (2015).

660 24. H. Iwakawa, A. Shinmyo, M. Sekine, Arabidopsis CDKA;1, a cdc2 homologue,
661 controls proliferation of generative cells in male gametogenesis. *The Plant Journal*
662 **45**, 819–831 (2006).

663 25. F. Alessi, S. Quarta, M. Savio, F. Riva, L. Rossi, L. A. Stivala, A. I. Scovassi, L.
664 Meijer, E. Prosperi, The Cyclin-Dependent Kinase Inhibitors Olomoucine and
665 Roscovitine Arrest Human Fibroblasts in G1 Phase by Specific Inhibition of CDK2
666 Kinase Activity. *Experimental Cell Research* **245**, 8–18 (1998).

667 26. N. Glab, B. Labidi, L.-X. Qin, C. Trehin, C. Bergounioux, L. Meijer, Olomoucine, an
668 inhibitor of the cdc2/cdk2 kinases activity, blocks plant cells at the G1 to S and G2 to
669 M cell cycle transitions. *FEBS Letters* **353**, 207–211 (1994).

670 27. R. Jhou, K. Sun, G. Sun, H. Wang, C. Chang, H. Huang, S. Lu, S. Tang, Inhibition of
671 cyclin-dependent kinases by olomoucine and roscovitine reduces
672 lipopolysaccharide-induced inflammatory responses via down-regulation of nuclear
673 factor κB. *Cell Prolif* **42**, 141–149 (2009).

674 28. J. Abramson, J. Adler, J. Dunger, R. Evans, T. Green, A. Pritzel, O. Ronneberger, L.
675 Willmore, A. J. Ballard, J. Bambrick, S. W. Bodenstein, D. A. Evans, C.-C. Hung, M.
676 O'Neill, D. Reiman, K. Tunyasuvunakool, Z. Wu, A. Žemgulytė, E. Arvaniti, C.
677 Beattie, O. Bertolli, A. Bridgland, A. Cherepanov, M. Congreve, A. I. Cowen-Rivers,
678 A. Cowie, M. Figurnov, F. B. Fuchs, H. Gladman, R. Jain, Y. A. Khan, C. M. R. Low,
679 K. Perlin, A. Potapenko, P. Savy, S. Singh, A. Stecula, A. Thillaisundaram, C. Tong,
680 S. Yakneen, E. D. Zhong, M. Zielinski, A. Žídek, V. Bapst, P. Kohli, M. Jaderberg, D.
681 Hassabis, J. M. Jumper, Accurate structure prediction of biomolecular interactions
682 with AlphaFold 3. *Nature* **630**, 493–500 (2024).

683 29. W. Lu, J. Zhang, W. Huang, Z. Zhang, X. Jia, Z. Wang, L. Shi, C. Li, P. G. Wolynes,
684 S. Zheng, DynamicBind: predicting ligand-specific protein-ligand complex structure
685 with a deep equivariant generative model. *Nat Commun* **15**, 1071 (2024).

686 30. M. J. Abraham, T. Murtola, R. Schulz, S. Páll, J. C. Smith, B. Hess, E. Lindahl,
687 GROMACS: High performance molecular simulations through multi-level parallelism
688 from laptops to supercomputers. *SoftwareX* **1–2**, 19–25 (2015).

689 31. E. C. Meng, T. D. Goddard, E. F. Pettersen, G. S. Couch, Z. J. Pearson, J. H.
690 Morris, T. E. Ferrin, UCSF ChimeraX: Tools for structure building and analysis.
691 *Protein Science* **32**, e4792 (2023).

692 32. J. Holcakova, P. Tomasec, J. J. Bugert, E. C. Wang, G. W. Wilkinson, R. Hrstka, V.
693 Krystof, M. Strnad, B. Vojtesek, The inhibitor of cyclin-dependent kinases,
694 olomoucine II, exhibits potent antiviral properties. *Antivir Chem Chemother* **20**, 133–
695 142 (2010).

696 33. Y. Sako, K. Ninomiya, Y. Okuno, M. Toyomoto, A. Nishida, Y. Koike, K. Ohe, I. Kii,
697 S. Yoshida, N. Hashimoto, T. Hosoya, M. Matsuo, M. Hagiwara, Development of an
698 orally available inhibitor of CLK1 for skipping a mutated dystrophin exon in
699 Duchenne muscular dystrophy. *Sci Rep* **7**, 46126 (2017).

700 34. M. Watt, K. Schneebeli, P. Dong, I. W. Wilson, The shoot and root growth of
701 Brachypodium and its potential as a model for wheat and other cereal crops.
702 *Functional Plant Biol.* **36**, 960–969 (2009).

703 35. V. Chochois, J. P. Vogel, M. Watt, Application of Brachypodium to the genetic
704 improvement of wheat roots. *Journal of Experimental Botany* **63**, 3467–3474 (2012).

705 36. V. Chochois, J. P. Vogel, G. J. Rebetzke, M. Watt, Variation in Adult Plant
706 Phenotypes and Partitioning among Seed and Stem-Borne Roots across
707 Brachypodium distachyon Accessions to Exploit in Breeding Cereals for Well-
708 Watered and Drought Environments. *Plant Physiology* **168**, 953–967 (2015).

37. T. M. Nolan, N. Vukašinović, C.-W. Hsu, J. Zhang, I. Vanhoutte, R. Shahan, I. W. Taylor, L. Greenstreet, M. Heitz, A. Afanassiev, P. Wang, P. Szekely, A. Brosnan, Y. Yin, G. Schiebinger, U. Ohler, E. Russinova, P. N. Benfey, Brassinosteroid gene regulatory networks at cellular resolution in the Arabidopsis root. *Science* **379**, eadf4721 (2023).

38. R. Shahan, C.-W. Hsu, T. M. Nolan, B. J. Cole, I. W. Taylor, L. Greenstreet, S. Zhang, A. Afanassiev, A. H. C. Vlot, G. Schiebinger, P. N. Benfey, U. Ohler, A single-cell Arabidopsis root atlas reveals developmental trajectories in wild-type and cell identity mutants. *Developmental Cell* **57**, 543-560.e9 (2022).

39. M. J. Jakoby, C. Weinl, S. Pusch, S. J. H. Kuijt, T. Merkle, N. Dissmeyer, A. Schnittger, Analysis of the Subcellular Localization, Function, and Proteolytic Control of the Arabidopsis Cyclin-Dependent Kinase Inhibitor ICK1/KRP1. *Plant Physiology* **141**, 1293–1305 (2006).

40. Y. Zhou, G. Li, F. Brandizzi, L. C. Fowke, H. Wang, The plant cyclin-dependent kinase inhibitor ICK1 has distinct functional domains for in vivo kinase inhibition, protein instability and nuclear localization. *The Plant Journal* **35**, 476–489 (2003).

41. S. Kumar, M. Suleski, J. M. Craig, A. E. Kasprowicz, M. Sanderford, M. Li, G. Stecher, S. B. Hedges, TimeTree 5: An Expanded Resource for Species Divergence Times. *Molecular Biology and Evolution* **39**, msac174 (2022).

42. J. D. Scharwies, T. Clarke, Z. Zheng, A. Dinneny, S. Birkeland, M. A. Veltman, C. J. Sturrock, J. Banda, H. H. Torres-Martínez, W. G. Viana, R. Khare, J. Kieber, B. K. Pandey, M. Bennett, P. S. Schnable, J. R. Dinneny, Moisture-responsive root-branching pathways identified in diverse maize breeding germplasm. *Science* **387**, 666–673 (2025).

43. P. Mehra, B. K. Pandey, D. Melebari, J. Banda, N. Leftley, V. Couvreur, J. Rowe, M. Anfang, H. De Gernier, E. Morris, C. J. Sturrock, S. J. Mooney, R. Swarup, C. Faulkner, T. Beeckman, R. P. Bhalerao, E. Shani, A. M. Jones, I. C. Dodd, R. E. Sharp, A. Sadanandom, X. Draye, M. J. Bennett, Hydraulic flux–responsive hormone redistribution determines root branching. *Science* **378**, 762–768 (2022).

44. B. K. Pandey, G. Huang, R. Bhosale, S. Hartman, C. J. Sturrock, L. Jose, O. C. Martin, M. Karady, L. A. C. J. Voesenek, K. Ljung, J. P. Lynch, K. M. Brown, W. R. Whalley, S. J. Mooney, D. Zhang, M. J. Bennett, Plant roots sense soil compaction through restricted ethylene diffusion. *Science* **371**, 276–280 (2021).

45. D. Shen, N. Micic, R. E. Venado, N. Bjarnholt, C. Crocoll, D. P. Persson, S. Samwald, S. Kopriva, P. Westhoff, S. Metzger, U. Neumann, R. T. Nakano, M. Marín Arancibia, T. G. Andersen, Apoplastic barriers are essential for nodule formation and nitrogen fixation in Lotus japonicus. *Science* **387**, 1281–1286 (2025).

46. C. Yang, K. Sofroni, E. Wijnker, Y. Hamamura, L. Carstens, H. Harashima, S. C. Stolze, D. Vezon, L. Chelysheva, Z. Orban-Nemeth, G. Pochon, H. Nakagami, P.

748 Schlögelhofer, M. Grelon, A. Schnittger, The Arabidopsis Cdk1/Cdk2 homolog
749 CDKA;1 controls chromosome axis assembly during plant meiosis. *The EMBO*
750 *Journal* **39**, e101625 (2020).

751 47. J. Schindelin, I. Arganda-Carreras, E. Frise, V. Kaynig, M. Longair, T. Pietzsch, S.
752 Preibisch, C. Rueden, S. Saalfeld, B. Schmid, J.-Y. Tinevez, D. J. White, V.
753 Hartenstein, K. Eliceiri, P. Tomancak, A. Cardona, Fiji: an open-source platform for
754 biological-image analysis. *Nat Methods* **9**, 676–682 (2012).

755 48. S. Chen, Y. Zhou, Y. Chen, J. Gu, fastp: an ultra-fast all-in-one FASTQ
756 preprocessor. *Bioinformatics* **34**, i884–i890 (2018).

757 49. D. Swarbreck, C. Wilks, P. Lamesch, T. Z. Berardini, M. Garcia-Hernandez, H.
758 Foerster, D. Li, T. Meyer, R. Muller, L. Ploetz, A. Radenbaugh, S. Singh, V. Swing,
759 C. Tissier, P. Zhang, E. Huala, The Arabidopsis Information Resource (TAIR): gene
760 structure and function annotation. *Nucleic Acids Research* **36**, D1009–D1014
761 (2008).

762 50. A. Dobin, C. A. Davis, F. Schlesinger, J. Drenkow, C. Zaleski, S. Jha, P. Batut, M.
763 Chaisson, T. R. Gingeras, STAR: ultrafast universal RNA-seq aligner. *Bioinformatics*
764 **29**, 15–21 (2013).

765 51. R. Patro, G. Duggal, M. I. Love, R. A. Irizarry, C. Kingsford, Salmon provides fast
766 and bias-aware quantification of transcript expression. *Nat Methods* **14**, 417–419
767 (2017).

768 52. M. I. Love, W. Huber, S. Anders, Moderated estimation of fold change and
769 dispersion for RNA-seq data with DESeq2. *Genome Biology* **15**, 550 (2014).

770 53. R: The R Project for Statistical Computing. https://www.r-project.org/.

771 54. pheatmap: Pretty Heatmaps version 1.0.12 from CRAN.
772 https://rdrr.io/cran/pheatmap/.

773 55. N. Michaud-Agrawal, E. J. Denning, T. B. Woolf, O. Beckstein, MDAnalysis: A toolkit
774 for the analysis of molecular dynamics simulations. *Journal of Computational*
775 *Chemistry* **32**, 2319–2327 (2011).

776 56. T. Senapathi, S. Bray, C. B. Barnett, B. Grüning, K. J. Naidoo, Biomolecular
777 Reaction and Interaction Dynamics Global Environment (BRIDGE). *Bioinformatics*
778 **35**, 3508–3509 (2019).

779
780
781
782
783
784

785 Figure 1

786

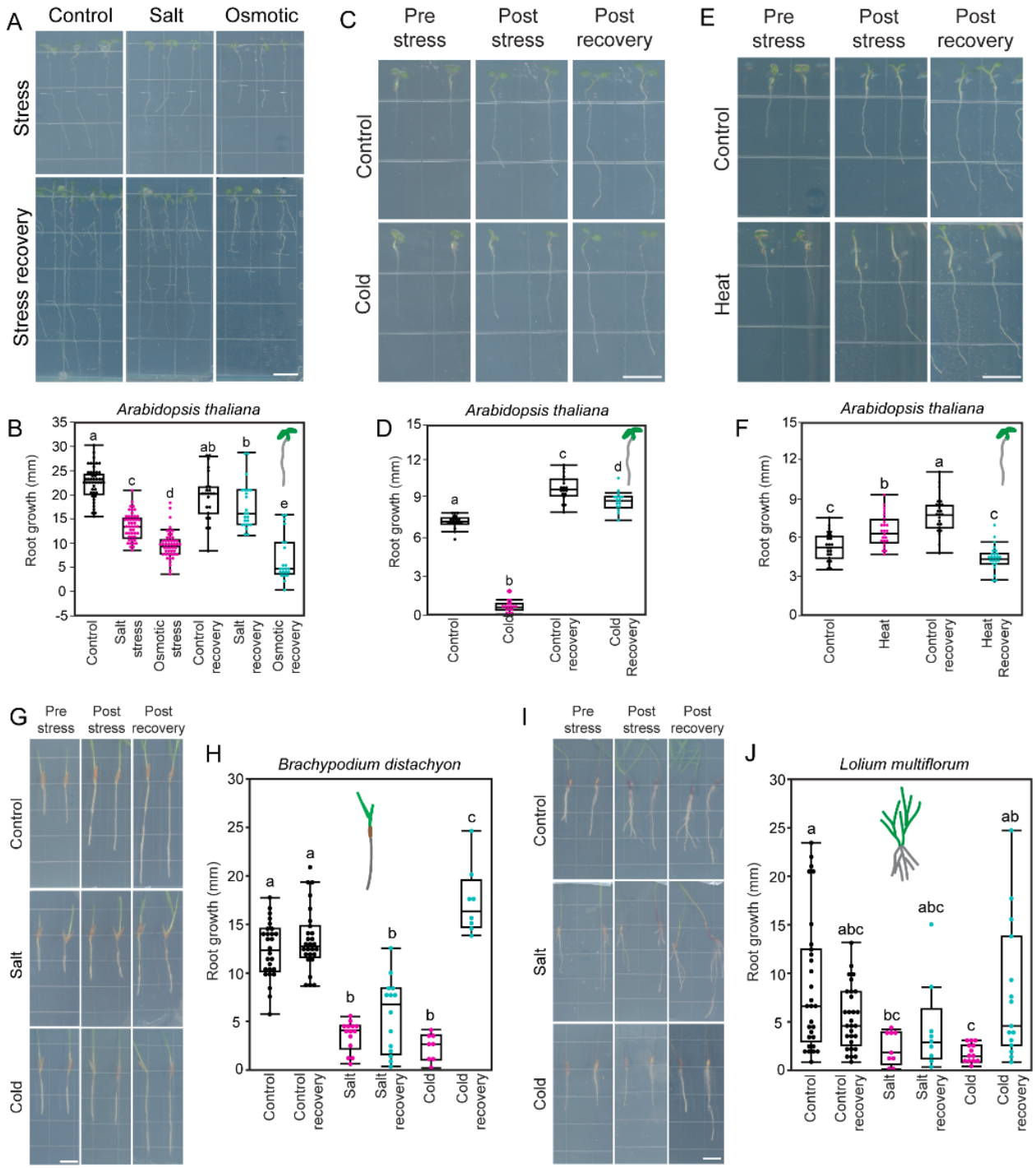

787

788

789

790

791

792

Figure 1: Environmental stress and stress recovery in Arabidopsis, Brachypodium, and annual ryegrass. (A) Root growth response of Arabidopsis in presence of salt and mannitol stress (upper panel) and recovery (lower panel). (B) Quantification of root growth from A. (C) Root growth response of Arabidopsis during pre- and post-cold stress, and post-cold stress recovery conditions. (D) Quantification of root growth from C. (E) Root growth response of Arabidopsis during pre- and post-heat stress, and post-heat stress recovery conditions. (F) Quantification of root growth from E. (G) Examples of root growth response of Brachypodium during salt and cold stress, and consequent recovery period. (H) Quantification of Brachypodium root growth in salt and cold stress and recovery experiments. (I) Examples of root growth response of annual ryegrass during salt and cold stress, and consequent recovery period. (J) Quantification of annual ryegrass root growth in salt and cold stress and recovery experiments. In panels A, C, E, G, and I, scale bar = 10 mm. Statistical test is performed based on Tukey's Honest test (B, D, F, H, and J). Groups labeled with the same letter are not statistically different from each other (alpha = 0.05). Boxplots show median values (center line), 25th to 75th interquartile range (box) and 1.5*interquartile range (whiskers) (B, D, F, H, and J).

Figure 2

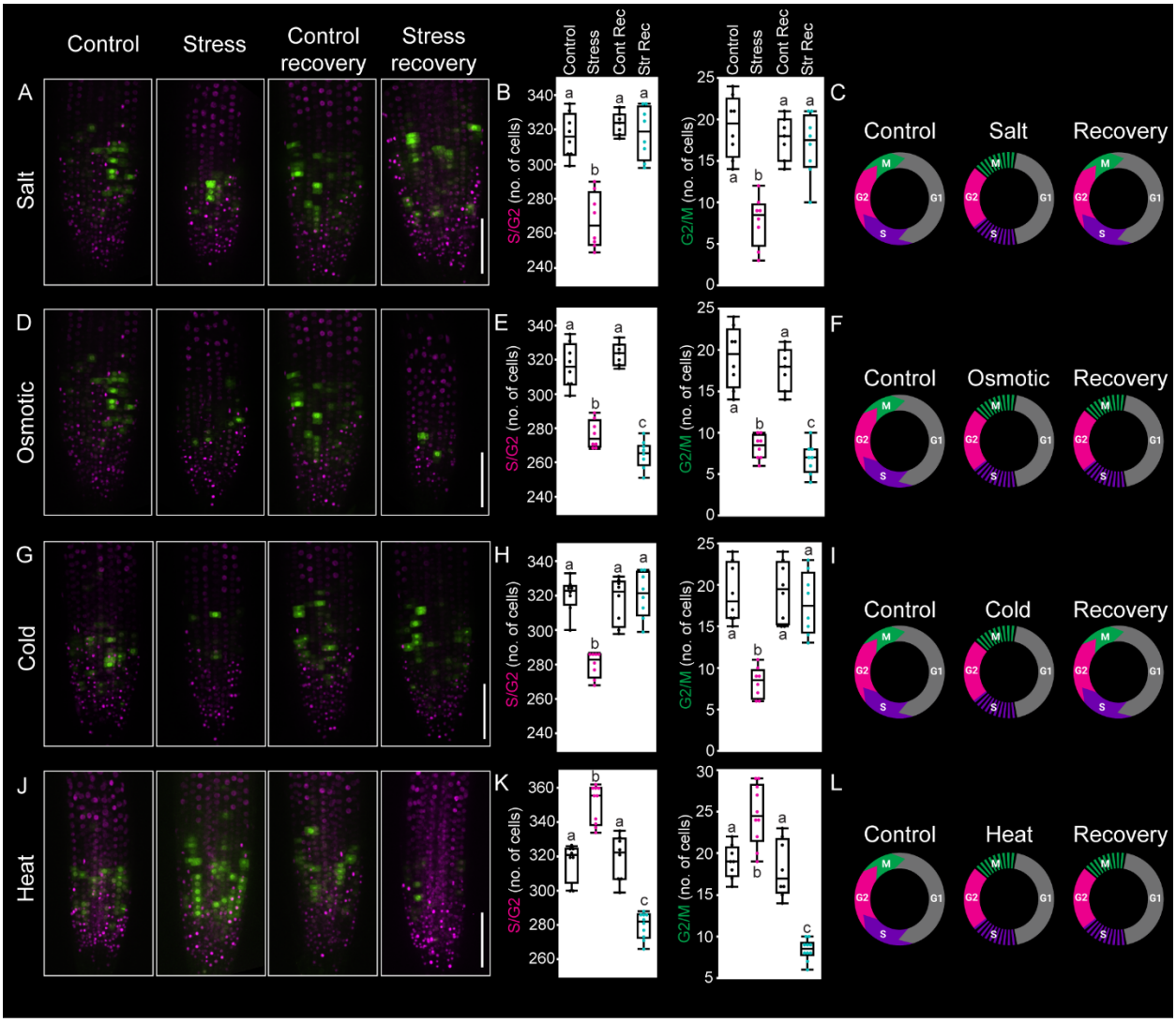

Figure 2: Response of cell cycle marker during environmental stress and stress recovery in Arabidopsis. Representative images of cell cycle marker Cytrap, quantification of S/G2 and G2/M phase specific cells, and cell cycle regulation model during salt (A-C), osmotic (D-F), cold (G-I), and heat (J-L) stress and recovery periods. Magenta and green indicate S/G2 and G2/M phase, respectively, specific cells. At least 8-10 roots were observed for each condition and the entire Z plane of the root meristem was considered to quantify the cells. Scale bar = 100 µm (A, D, G, and J). Statistical test is performed based on Tukey's Honest test (B, E, H, and K). Groups labeled with the same letter are not statistically different from each other (alpha = 0.05). Boxplots show median values (center line), 25th to 75th interquartile range (box) and 1.5*interquartile range (whiskers) (B, E, H, and K).

Figure 3

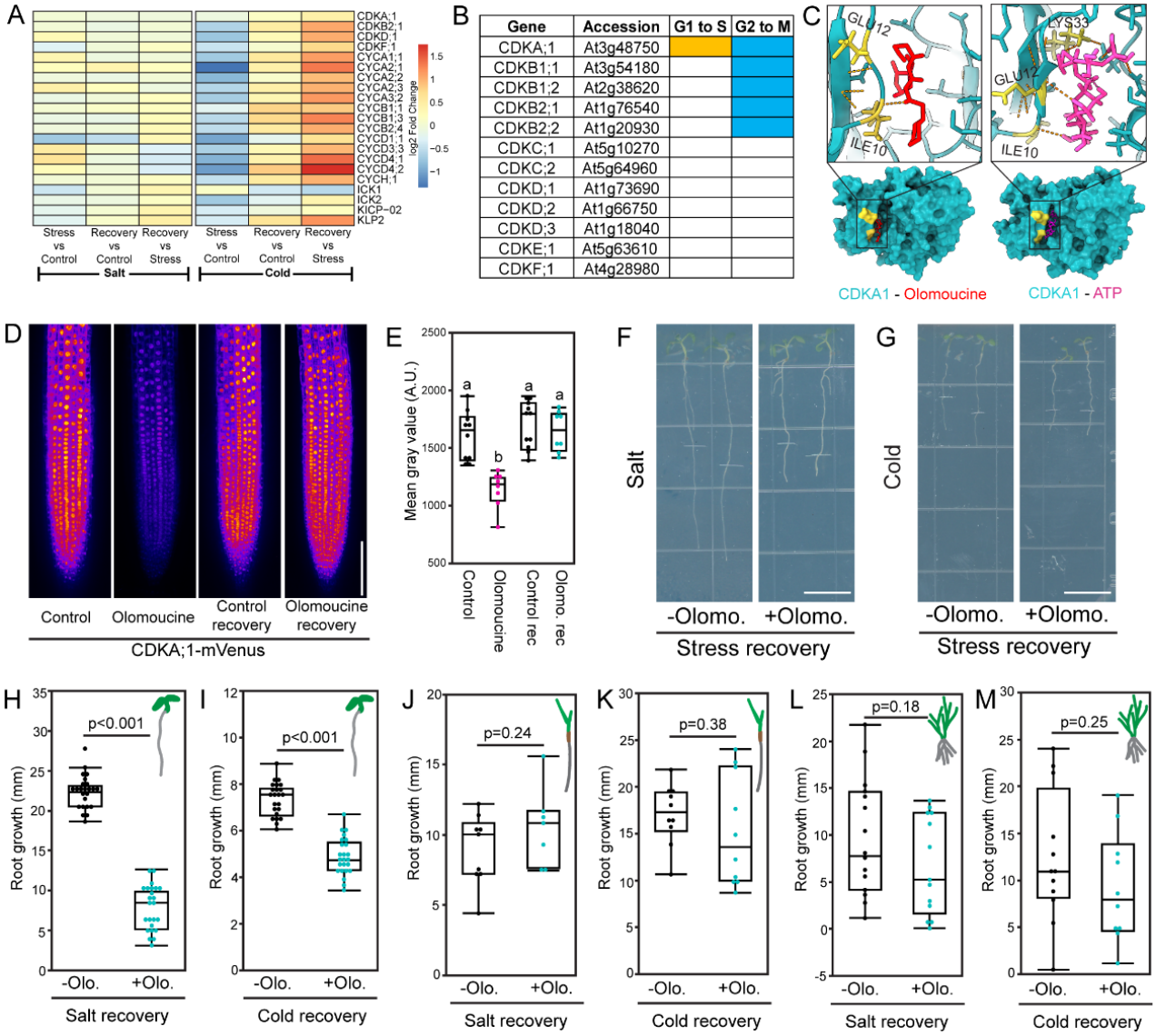

Gene	Accession	G1 to S	G2 to M
CDKA;1	At3g48750		
CDKB1;1	At3g54180		
CDKB1;2	At2g38620		
CDKB2;1	At1g76540		
CDKB2;2	At1g20930		
CDKC;1	At5g10270		
CDKC;2	At5g64960		
CDKD;1	At1g73690		
CDKD;2	At1g66750		
CDKD;3	At1g18040		
CDKE;1	At5g63610		
CDKF;1	At4g28980		

Figure 3: Intact G1 to S and G2 to M transitions are required for salt and cold stress recovery. (A) Relative expression of a sub-set of core cell cycle genes during the salt and cold stress, and subsequent recovery periods. (B) List of Arabidopsis CDKs involved in G1 to S (yellow) and G2 to M (cyan) transitions. (C) *In silico* interaction assay of olomoucine (left, red) and ATP (right, magenta) with CDKA1 (cyan). Interacting amino acids were highlighted in yellow. (D) CDKA;1-mVenus signal in presence of olomoucine and the recovery period. (E) Quantification of mean gray value from D. Salt (F) and cold (G) stress recovery in presence of olomoucine in Arabidopsis. Quantification of salt (H) and cold (I) stress recovery in presence of olomoucine from F and G, respectively. Salt (J) and cold (K) stress recovery in presence of olomoucine in Brachypodium. Salt (L) and cold (M) stress recovery in presence of olomoucine in annual ryegrass. Scale bar = 100 µm (D) and 10 mm (F and G). (E) Statistical test is performed based on Tukey's Honest test. Groups labeled with the same letter are not statistically different from each other (alpha = 0.05). Boxplots show median values (center line), 25th to 75th interquartile range (box) and 1.5*interquartile range (whiskers). Student's t-test was performed for H, I, J, K, L, and M.

Figure 4

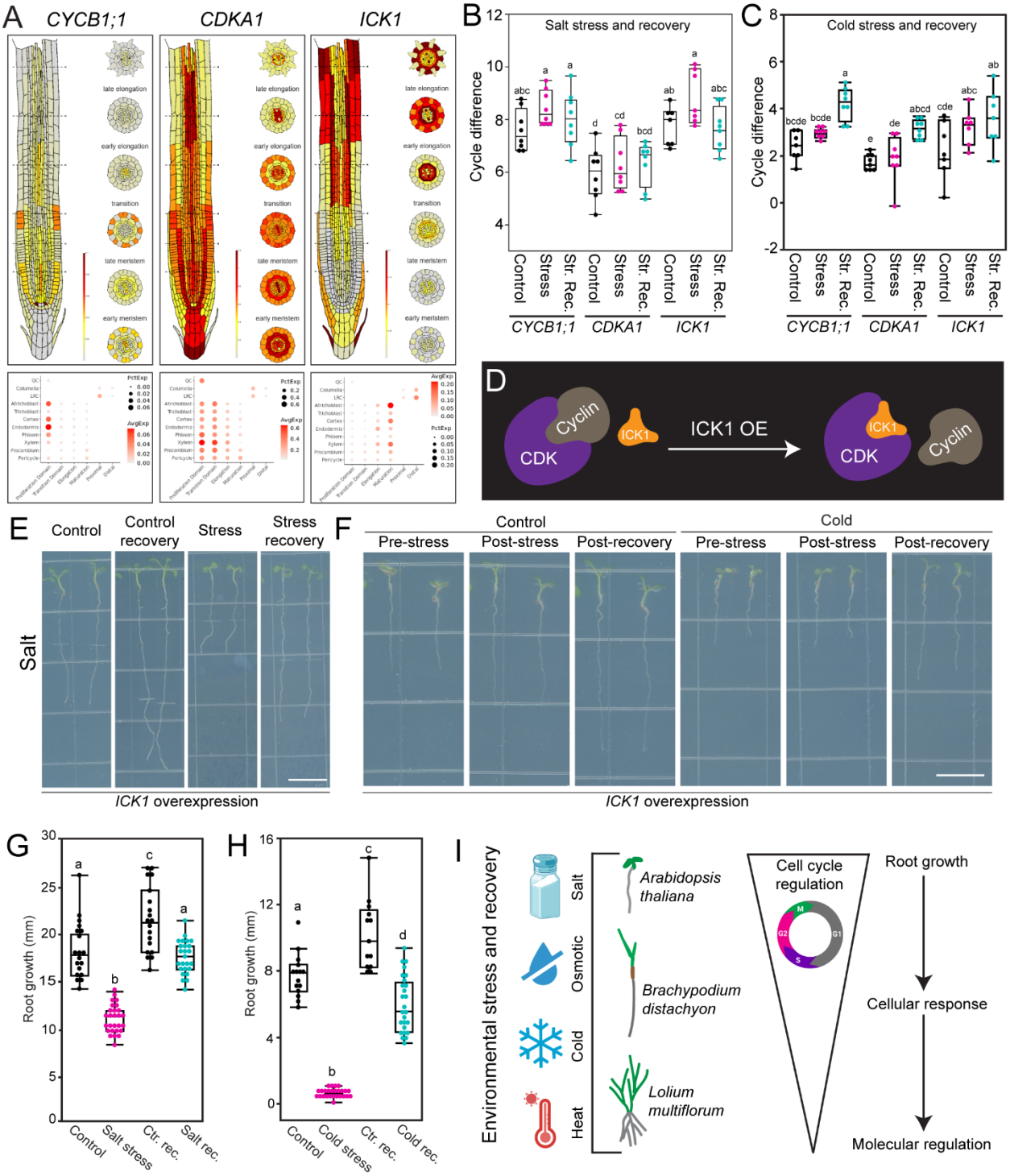
A
CYCB1;1
CDKA1
ICK1
late elongation
early elongation
transition
late meristem
early meristem
B
Salt stress and recovery
Cycle difference
Control
Stress
Str. Rec.
CYCB1;1
CDKA1
ICK1
C
Cold stress and recovery
D
Cyclin
CDK
ICK1
ICK1 OE
E
Control
Control recovery
Stress
Stress recovery
Salt
ICK1 overexpression
F
Control
Cold
Pre-stress
Post-stress
Post-recovery
ICK1 overexpression
G
Root growth (mm)
Control
Salt stress
Ctr. rec.
Salt rec.
H
Root growth (mm)
Control
Cold stress
Ctr. rec.
Cold rec.
I
Environmental stress and recovery
Salt
Osmotic
Cold
Heat
Arabidopsis thaliana
Brachypodium distachyon
Lolium multiflorum
Cell cycle regulation
Root growth
Cellular response
Molecular regulation

Figure 4: CDKA1-dependent cell cycle transitions are required for salt and cold stress recovery. (A) Single cell sequencing data for demonstrating the spatial expression pattern of *CYCB1;1* (left), *CDKA1* (middle), and *ICK1* (right). The upper panel highlights a color based gradient for longitudinal expression pattern and the lower panel highlights the expression pattern in a dot plot manner. Real time PCR of *CYCB1;1* (left), *CDKA1* (middle), and *ICK1* (right) genes in salt (B) and cold (C) stress, and corresponding recovery periods. (D) Schematic model of ICK1 overexpression based CDK inhibition. Salt (E) and cold (F) recovery response of ICK1 overexpression line in Arabidopsis. Quantification of root growth response of ICK1 overexpression line during salt (G) and cold (H) stress and recovery from E and F, respectively. (I) Graphical model highlights the summarized version of the study, where Arabidopsis, Brachypodium, and annual ryegrass were tested for multiple stress, and stress recovery focusing on cell cycle regulation at organ or root growth, cellular, and molecular scale. Scale bar = 10 mm (E and F). Statistical test is performed based on Tukey's Honest test (B, C, G, and H). Groups labeled with the same letter are not statistically different from each other (alpha = 0.05). Boxplots show median values (center line), 25th to 75th interquartile range (box) and 1.5*interquartile range (whiskers) (B, C, G, and H).

Supplemental figure 1

Organism	Stress	Condition	Transfer	Stress	Recovery
Arabidopsis thaliana	Salt	100mM NaCl	4DPG	6DPG	8DPG
Arabidopsis thaliana	Osmotic	300mM Mannitol	4DPG	6DPG	8DPG
Arabidopsis thaliana	Cold	4°C	4DPG	5DPG	6DPG
Arabidopsis thaliana	Heat	29°C	4DPG	5DPG	6DPG
Brachypodium distachyon	Salt	200mM NaCl	2DPG	4DPG	6DPG
Brachypodium distachyon	Cold	4°C	2DPG	4DPG	6DPG
Lolium multiflorum	Salt	200mM NaCl	2DPG	4DPG	6DPG
Lolium multiflorum	Cold	4°C	2DPG	4DPG	6DPG

Supplemental figure 1: Experimental conditions for Arabidopsis, Brachypodium, and annual ryegrass. Concentration of salt and mannitol, temperature for cold and heat stress, and developmental stage of root, and incubation periods were mentioned for each individual stress and each organism used in this study.

Supplemental figure 2

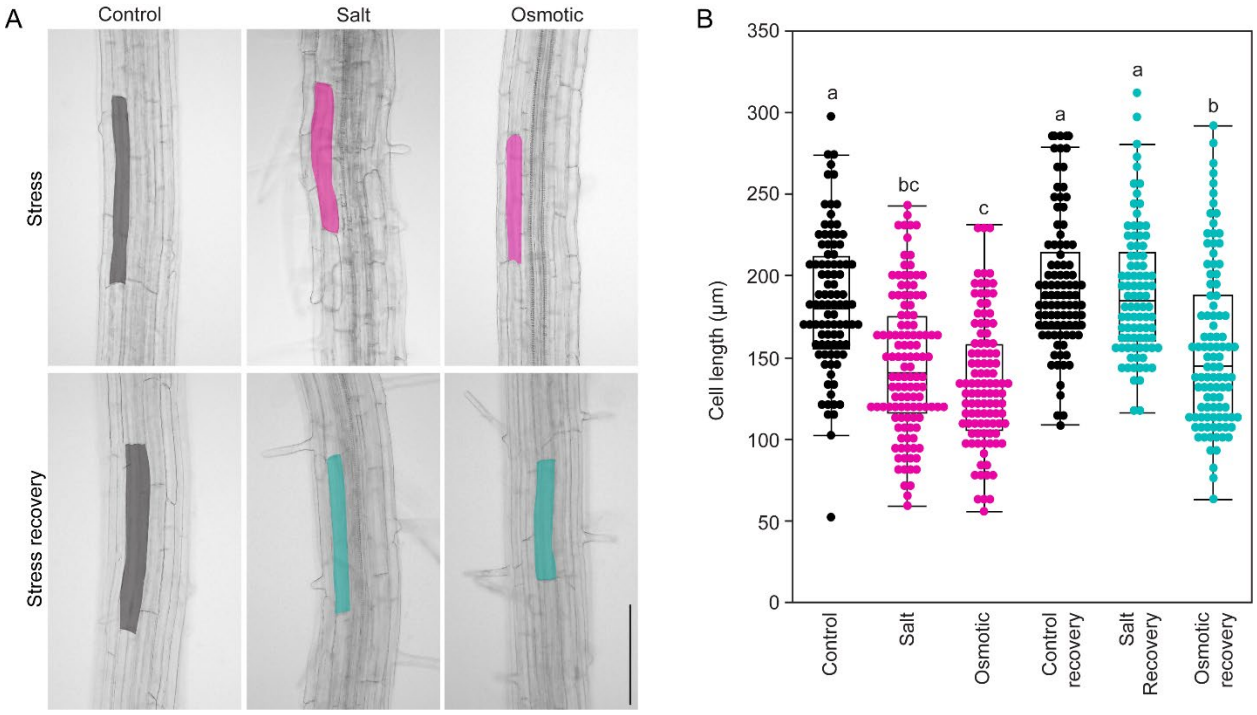

Supplemental figure 2: Cell elongation during salt and osmotic stress, and stress recovery period. (A) Epidermal cell length was measured during the control, salt and osmotic stress, and corresponding recovery period. Scale bar = 100 µm. (B) Quantification of cell length from A. Statistical test is performed based on Tukey's Honest test. Groups labeled with the same letter are not statistically different from each other (alpha = 0.05). Boxplots show median values (center line), 25th to 75th interquartile range (box) and 1.5*interquartile range (whiskers).

Supplemental figure 3

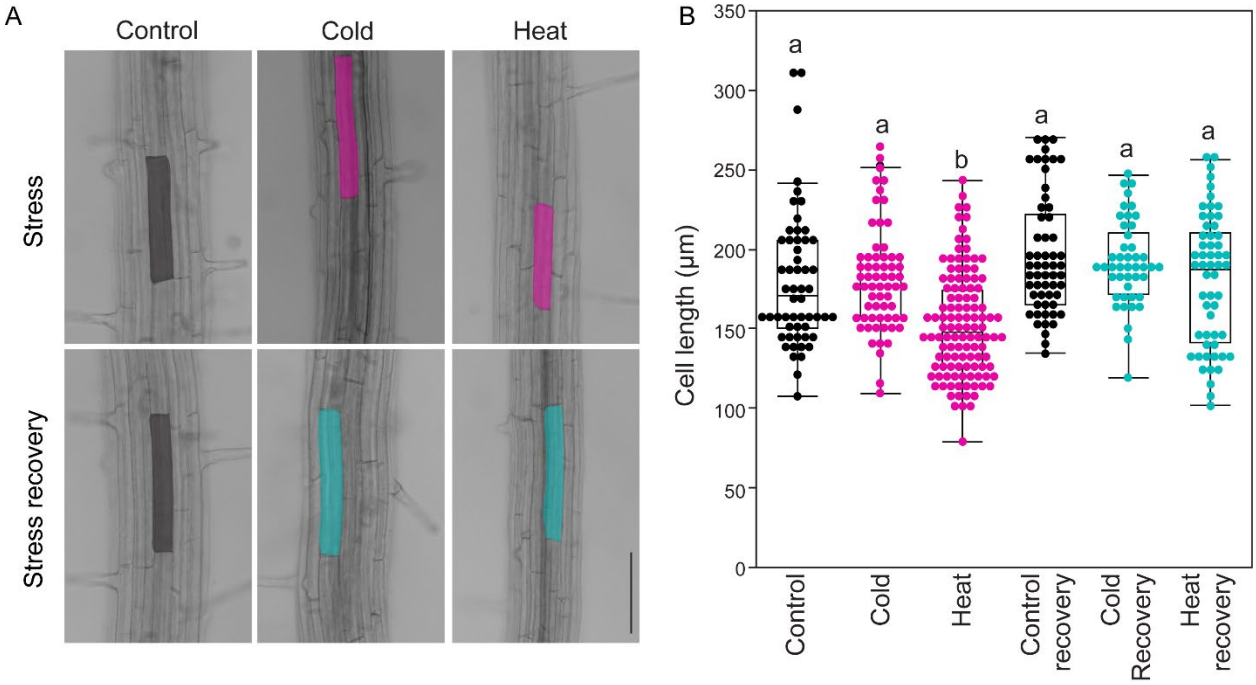

Supplemental figure 3: Cell elongation during cold and heat stress, and stress recovery period. (A) Epidermal cell length was measured during the control, cold and heat stress, and corresponding recovery period. Scale bar = 100 µm. (B) Quantification of cell length from A. Statistical test is performed based on Tukey's Honest test. Groups labeled with the same letter are not statistically different from each other (alpha = 0.05). Boxplots show median values (center line), 25th to 75th interquartile range (box) and 1.5*interquartile range (whiskers).

Supplemental figure 4

	Stress condition		Recovery condition	
	Cell division	Cell elongation	Cell division	Cell elongation
Salt	↓	↓	✓	✓
Mannitol	↓	↓	X	X
Cold	↓	-	✓	-
Heat	↑	↓	X	-

Supplemental figure 4: Summary of cell division and cell elongation during salt, osmotic, cold, and heat stress, and stress recovery period. The summary is based on Figure 1, 2, and Supplemental figure 2, 3. Upward and downward arrow during stress condition indicates increased cell division or cell elongation. Dash line indicates neutral or wild-type response to the stress. Tick and cross marks indicate recovered and not recovered cell division or cell elongation during the recovery period. Dash line indicates neutral or wild-type response during the recovery period.

Supplemental figure 5

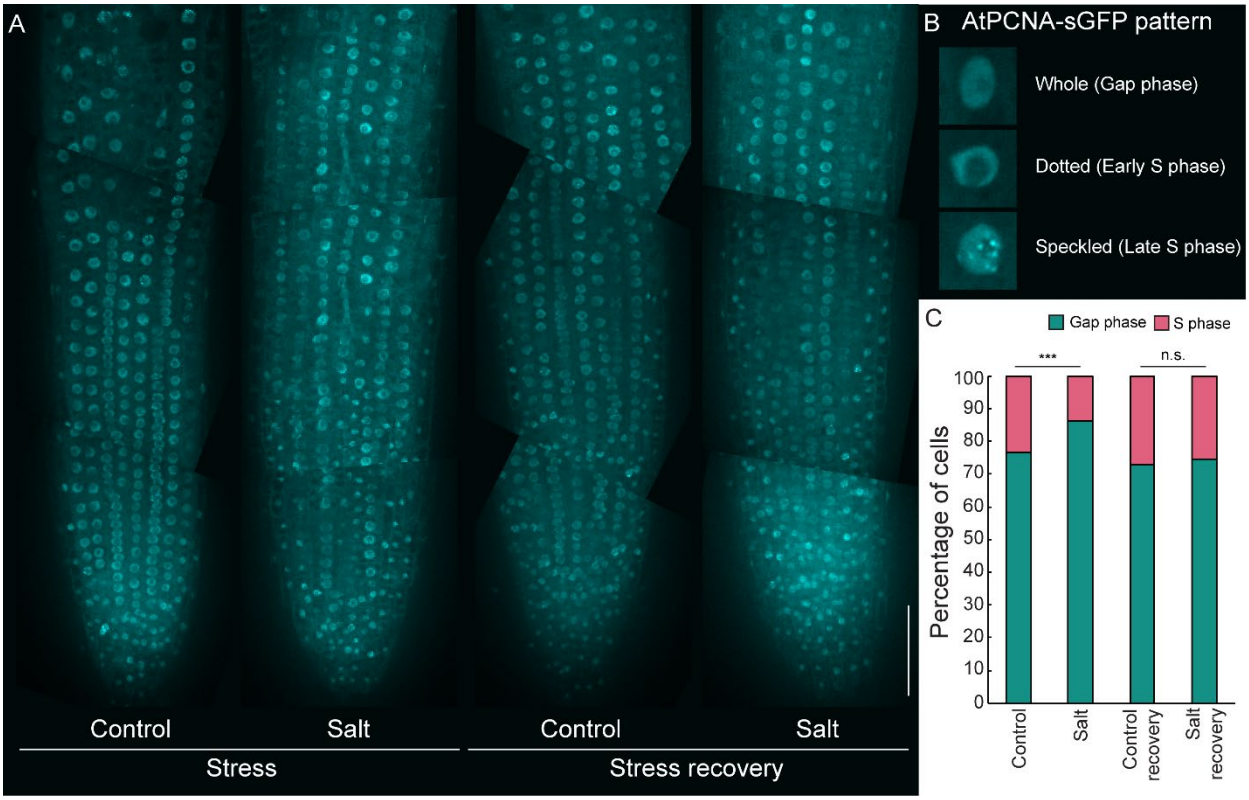

Supplemental figure 5: PCNA-GFP signal during salt stress and recovery. (A) Cell cycle marker PCNA-GFP signal during salt stress and recovery. Scale bar = 100 µm. (B) Characteristic pattern of whole (Gap phase), dotted (early S phase), and speckled (late S phase) pattern of PCNA-GFP marker. (C) Quantification of number of cells in gap phase and S phase during salt stress and recovery. Statistical test was performed based on Fisher's exact test.

Supplemental figure 6

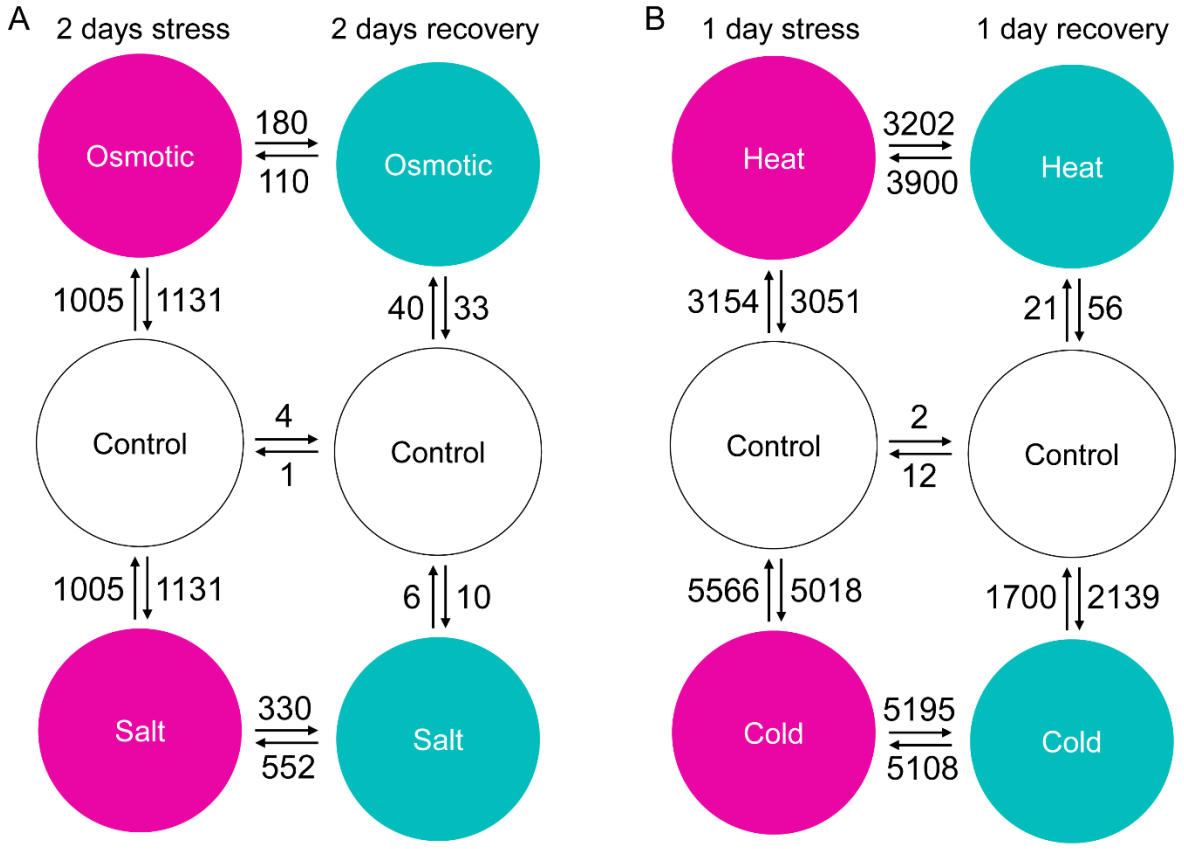

Supplemental figure 6: Differential gene expression from comparative transcriptomics. Number of differentially expressed genes during stress [salt (A), osmotic (A), cold (B), and heat (B)] and stress recovery are highlighted.

1154 Supplemental figure 7
1155

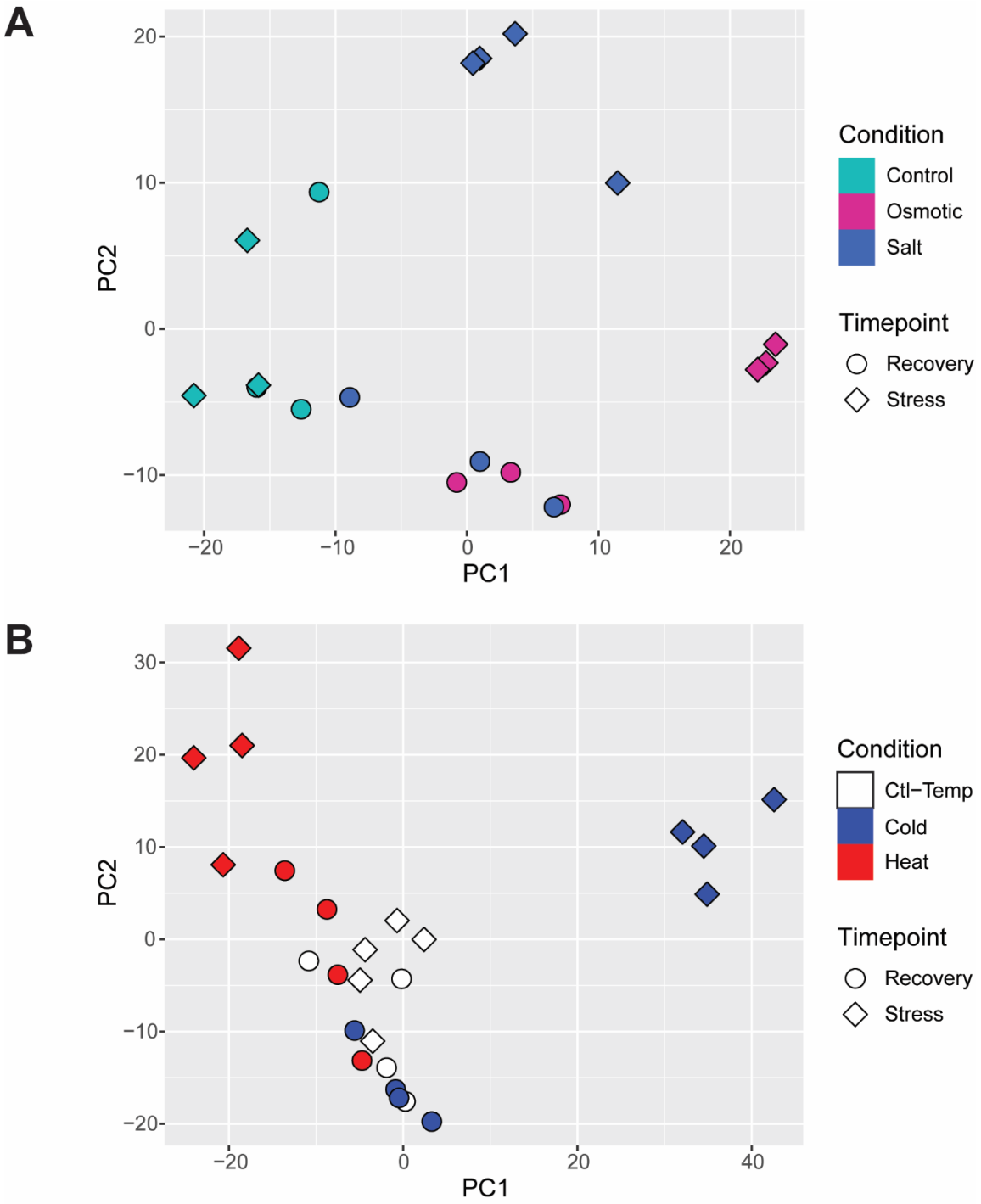

1156
1157
1158
1159 **Supplemental figure 7:** Principal component analysis (PCA) of RNAseq samples. PCA
1160 demonstrates the clustering of similar RNAseq samples for control, stress, control
1161 recovery, and stress recovery in A (salt and osmotic stress) and B (cold and heat
1162 stress).

Supplemental figure 8

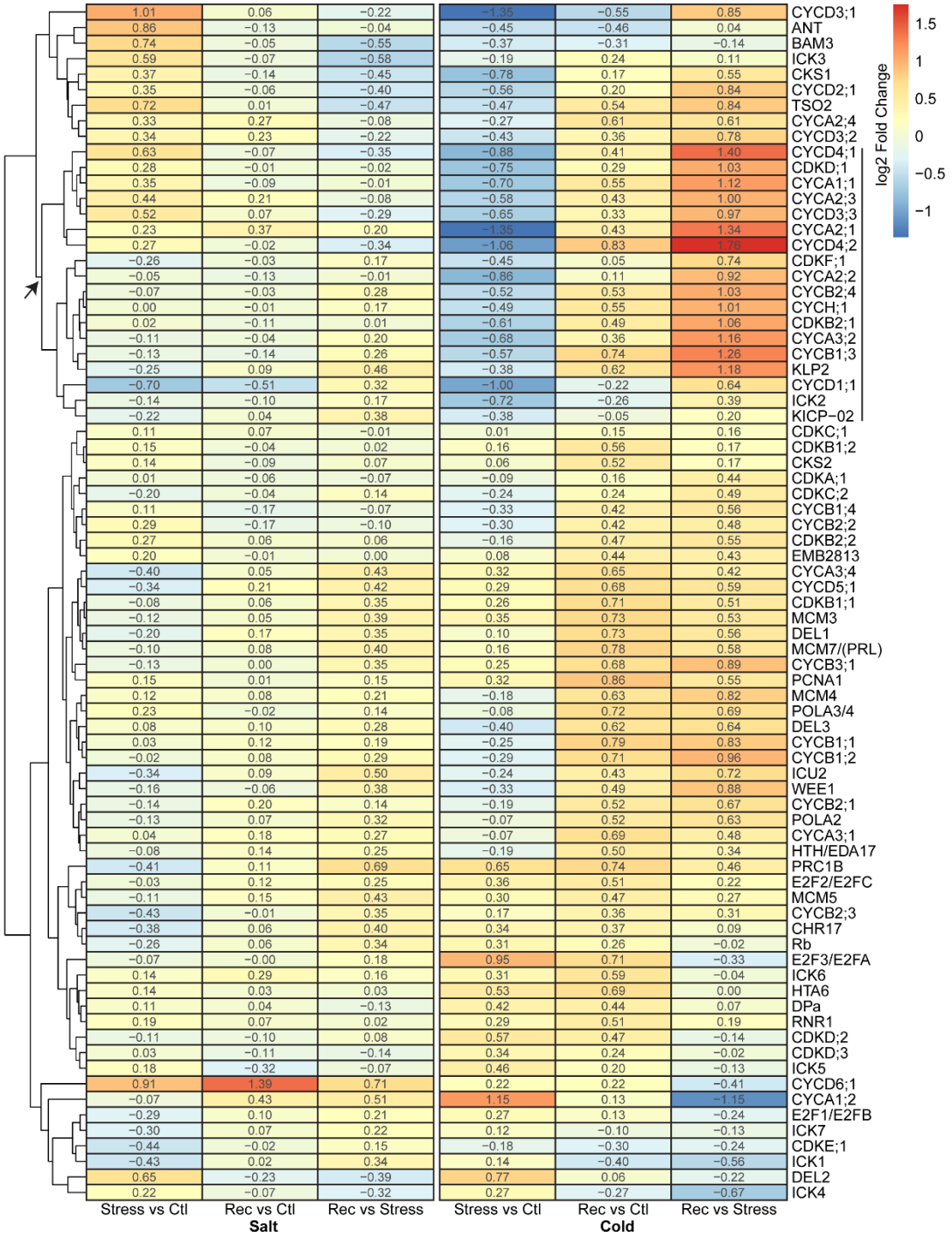

Supplemental figure 8: Differential expression of core cell cycle genes in Arabidopsis. Log2Fold changes of core cell cycle genes based on the comparative transcriptomics during salt and cold stress, and stress recovery. The gene clustering highlights a subset of genes used in Figure 3A.

1172 Supplemental figure 9
1173

Gene	Accession	G1 to S	G2 to M
CDKA;1	At3g48750		
CDKB1;1	At3g54180		
CDKB1;2	At2g38620		
CDKB2;1	At1g76540		
CDKB2;2	At1g20930		
CDKC;1	At5g10270		
CDKC;2	At5g64960		
CDKD;1	At1g73690		
CDKD;2	At1g66750		
CDKD;3	At1g18040		
CDKE;1	At5g63610		
CDKF;1	At4g28980		

Gene	Accession	G1 to S	G2 to M
CYCA1;1	At1g44110		
CYCA1;2	At1g77390		
CYCA2;1	At5g25380		
CYCA2;2	At5g11300		
CYCA2;3	At1g15570		
CYCA2;4	At1g80370		
CYCA3;1	At5g43080		
CYCA3;2	At1g47210		
CYCA3;3	At1g47220		
CYCA3;4	At1g47230		
CYCB1;1	At4g37490		
CYCB1;2	At5g06150		
CYCB1;3	At3g11520		
CYCB1;4	At2g26760		
CYCB2;1	At2g17620		
CYCB2;2	At4g35620		
CYCB2;3	At1g20610		
CYCB2;4	At1g76310		
CYCB3;1	At1g16330		
CYCC1;1	At5g48640		
CYCC1;2	At5g48630		
CYCD1;1	At1g70210		
CYCD2;1	At2g22490		
CYCD3;1	At4g34160		
CYCD3;2	At5g67260		
CYCD3;3	At3g50070		
CYCD4;1	At5g65420		
CYCD4;2	At5g10440		
CYCD5;1	At4g37630		
CYCD6;1	At4g03270		
CYCD7;1	At5g02110		
CYCH;1	At5g27620		

1174
1175
1176
1177 **Supplemental figure 9:** Cell cycle specific function of CDKs and cyclins. List of
1178 Arabidopsis CDKs and cyclins involved in G1 to S (yellow) and G2 to M (cyan)
1179 transitions.
1180
1181
1182
1183

Supplemental figure 10

A

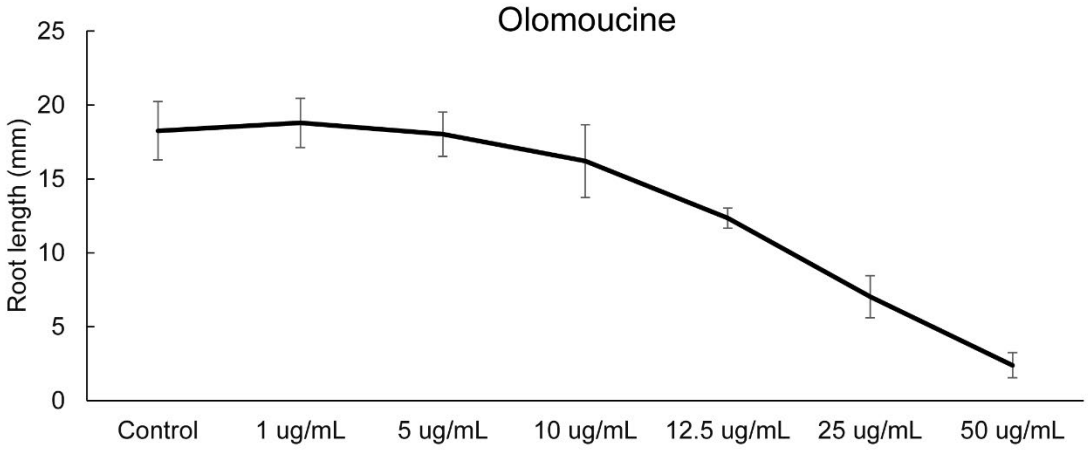

B

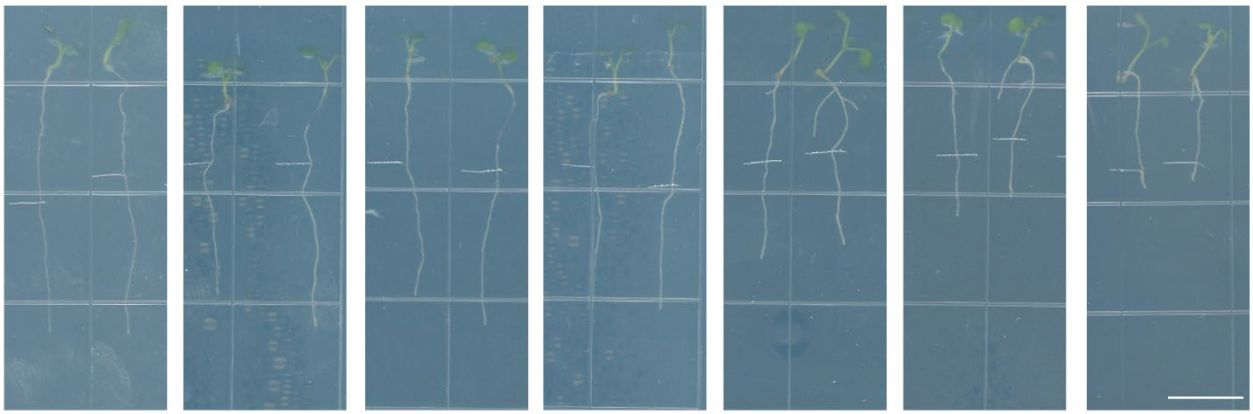

Control 1 µg/ml 5 µg/ml 10 µg/ml 12.5 µg/ml 25 µg/ml 50 µg/ml

Supplemental figure 10: Dose response curve of olomoucine. (A) Quantification of root length in presence of 1, 5, 10, 12.5, 25, and 50 µg/ml olomoucine. (B) Representative images for each olomoucine concentration corresponding to A. Scale bar = 10 mm.

1203 Supplemental figure 11
1204

CDKA1 and ATP			CDKA1 and olomoucine		
Donor	**Acceptor**	**H bond occupancy**	**Donor**	**Acceptor**	**H bond occupancy**
ATP-Side	ILE10-Main	14.69%	Olo-Side	ILE10-Main	9.49%
ATP-Side	GLU12-Main	4.45%	Olo-Side	GLU12-Main	0.35%
GLU12-Main	ATP-Side	0.20%	GLU12-Main	Olo-Side	3.95%
ATP-Side	ASP146-Main	2.10%	\	\	\
ATP-Side	ASP146-Side	76.27%	Olo-Side	ASP146-Side	0.35%

1205
1206
1207 **Supplemental figure 11:** Hydrogen bond occupancy of ATP and olomoucine with
1208 CDKA1. Interacting amino acids responsible for maintaining interaction with CDKA1 for
1209 both ATP and olomoucine; and hydrogen bond occupancy for each interaction.